JCIM JOURNAL OF CHEMICAL INFORMATION AND MODELING

pubs.acs.org/jcim Article

Umbrella Sampling Simulations Measure Switch Peptide Binding and Hydrophobic Patch Opening Free Energies in Cardiac Troponin

Austin M. Cool and Steffen Lindert*

Cite This: J. Chem. Inf. Model. 2022, 62, 5666−5674 Read Online

ACCESS | Metrics & More | Article Recommendations | Supporting Information

ABSTRACT: The cardiac troponin (cTn) complex is an important regulatory protein in heart contraction. Upon binding of Ca^{2+}, cTn undergoes a conformational shift that allows the troponin I switch peptide ($cTnI_{SP}$) to be released from the actin filament and bind to the troponin C hydrophobic patch ($cTnC_{HP}$). Mutations and modifications to this complex can change its sensitivity to Ca^{2+} and alter the energetics of the transition from the Ca^{2+}-unbound, $cTnI_{SP}$-unbound form to the Ca^{2+}-bound, $cTnI_{SP}$-bound form. We utilized targeted molecular dynamics (TMD) to obtain a trajectory of this transition pathway, followed by umbrella sampling to estimate the free energy associated with the $cTnI_{SP}$−$cTnC_{HP}$ binding and the $cTnC_{HP}$ opening events for wild-type (WT) cTn. We were able to reproduce experimental values for the $cTnI_{SP}$−$cTnC_{HP}$ binding event and obtain $cTnC_{HP}$ opening free energies in agreement with previous computational measurements of smaller cTnC systems. This excellent agreement for WT cTn demonstrated the strength of computational methods in studying the dynamics and energetics of the cTn complex. We then introduced mutations to the cTn complex that cause cardiomyopathy or alter its Ca^{2+} sensitivity and observed a general decrease in the free energy of opening the $cTnC_{HP}$. For these same mutations, we observed no general trend in the effect on the $cTnI_{SP}$−$cTnC_{HP}$ binding event. Our method sets the stage for future computational studies on this system that predict the consequences of yet uncharacterized mutations on cTn dynamics and energetics.

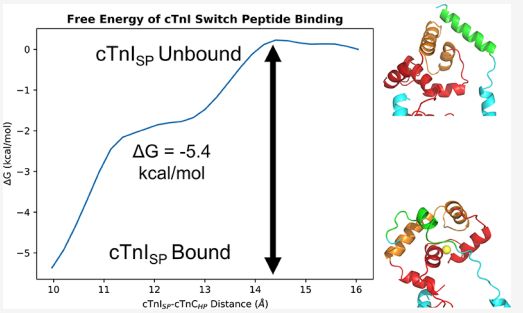

INTRODUCTION

Contraction of the thin filament in the heart muscle is regulated by Ca^{2+} binding to the cardiac isoform of the troponin (cTn) complex.[1] Upon binding of Ca^{2+} to cTn, a conformational shift occurs that releases cTn from actin, exposing myosin binding sites that allow muscle contraction to occur. The exact mechanism of the cTn conformational transition and how cTn mutations affect this process is still not fully understood.

The cTn complex is comprised of three subunits: the Ca^{2+}-binding subunit (cTnC), the inhibitory subunit (cTnI), and the tropomyosin-binding structural subunit (cTnT) (Figure 1). cTnC can be divided in two regions: N-terminal cTnC (NcTnC, residues 1−89) contains Ca^{2+} binding sites I and II, and C-terminal cTnC (CcTnC, residues 90−161) contains Ca^{2+} binding sites III and IV. Under normal physiological conditions, sites III and IV are always occupied, and site I is never occupied by Ca^{2+}. Thus, site II of NcTnC is predominately responsible for sensing Ca^{2+} for muscle contraction. When Ca^{2+} binds to site II, it induces a conformational and dynamical shift that exposes a hydrophobic patch ($cTnC_{HP}$) in NcTnC that is able to bind the cTnI switch peptide ($cTnI_{SP}$, residues 149−164). The $cTnI_{SP}$ (along with the cTnI inhibitory peptide) interacts with actin in the Ca^{2+}-unbound state, and its dissociation from actin and subsequent binding to the $cTnC_{HP}$ in the cTn Ca^{2+}-bound state allow for the thin filament interaction with myosin necessary for muscle contraction.

Mutations throughout the cTn complex subunits have been shown to cause cardiomyopathy, a disease that can lead to heart failure or sudden cardiac death.[2] Three types of cardiomyopathy caused by these mutations include hypertrophic (HCM), restrictive (RCM), and dilated (DCM). HCM causes thickening of the interventricular septum, leading to decreased ventricular filling and impaired diastolic function of the heart. RCM is a rarer disease but causes similar problems with decreased ventricular filling without thickening of the heart muscle. Both HCM and RCM mutations have been shown to increase Ca^{2+} sensitivity in cTnC. DCM has been shown to decrease cTnC Ca^{2+} sensitivity, with physiological effects including an increase in the size of the left ventricle, or both ventricles, and impaired systolic function.[3]

Received: April 27, 2022
Published: October 25, 2022

https://doi.org/10.1021/acs.jcim.2c00508
J. Chem. Inf. Model. 2022, 62, 5666−5674

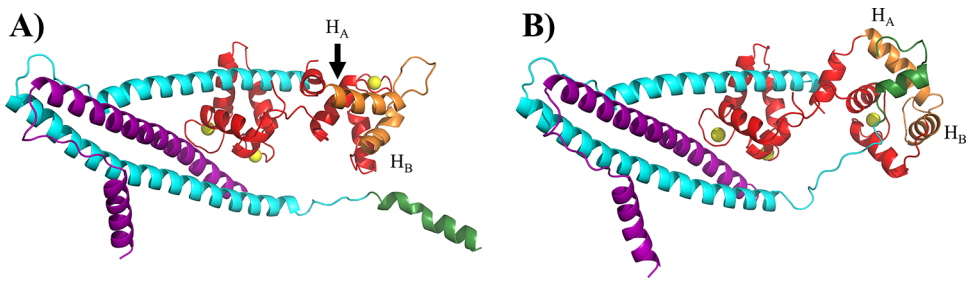

Figure 1. Cartoon representation of the cTn complex. A) TMD starting model representing Ca^{2+}-unbound, $cTnI_{SP}$-unbound cTn (PDB: 6KN7, chains a, b, and c). B) TMD final model representing Ca^{2+}-bound, $cTnI_{SP}$-bound cTn (PDB: 6KN8, chains a, b, and c). cTnT is depicted in purple, cTnI is cyan, and cTnC is red. Helices A and B (residues 14−48, $cTnC_{HP}$) of cTnC are shown in orange and labeled H_A and H_B, respectively. The $cTnI_{SP}$ (cTnI residues 149−164) are shown in green. Ca^{2+} ions added by AutoDock Vina are yellow.

Structurally, cTn has been well characterized. A partial crystal structure of the Ca^{2+}-bound cTn complex, published by Takeda et al.[4] in 2003, constituted a major advancement of our structural understanding of the complex. More recently, a cryo-EM structure of the entire cTn complex in the context of the thin filament was published by Yamada et al.[5] This study was able to elucidate structures of the cTn complex, anchored onto the thin filament, in the Ca^{2+}-bound and Ca^{2+}-unbound states. Although this breakthrough was able to provide snapshots of the cTn complex and thin filament in both states, it was unable to provide information on the conformational transition and thermodynamic pathway between the two. A quantitative assessment of these processes is desirable for our understanding of heart muscle biology and disease, drug discovery, and protein design.

Computational methods can facilitate the study of these processes.[6] Previous efforts have been able to utilize molecular dynamics (MD) and free energy methods to study Ca^{2+} binding to cTnC site II.[7−11] MD methods have also been able to investigate disruptions in dynamics upon the introduction of mutations that alter site II's Ca^{2+} sensitivity or mutations that have been linked with disease.[12−14] Enhanced sampling methods, umbrella sampling (US), and long timescale simulations have been utilized to study the energetic pathway for the transition between Ca^{2+}-unbound and Ca^{2+}-bound forms.[15−18] Simulations have also incorporated cTnI into the system to elucidate how other subunits in the cTn complex can affect the dynamics of cTnC.[19−24] Computer-aided drug discovery has also proven effective in helping identify potential therapeutics for heart disease by targeting the cTn complex.[25−29]

How mutations located in regions not involved in either the coordination of Ca^{2+} to site II or the $cTnI_{SP}$−$cTnC_{HP}$ binding event can alter the overall dynamics of muscle contraction remains underexplored. One hypothesis on how some of these mutations, particularly those in the cTnI inhibitory peptide ($cTnI_{IP}$), may affect troponin function was that they alter the availability, or effective concentration, of the $cTnI_{SP}$ to the $cTnC_{HP}$. Our lab previously explored this hypothesis by determining the volume sampled by the $cTnI_{SP}$ during MD simulations. We saw no significant difference in $cTnI_{SP}$ effective concentration between wild type (WT) and mutations in the cTnI inhibitory peptide (residues 137−148),[19] leading us to search for other computational methods to explore the effects of mutations on cTnC dynamics.

Another interesting interaction that has been, at least computationally, underexplored is the binding of the $cTnI_{SP}$ to the $cTnC_{HP}$ region. Experimentally, this has been studied before by Li et al.[30] in an NMR kinetic study of $cTnI_{147−163}$ titrated into a Ca^{2+}-bound NcTnC. The authors estimated a binding K_D of 154 μM.[30] Another experiment by Tikunova et al. estimated the binding affinity to be 200 nM using IAANS fluorescence,[31] measuring an almost three orders of magnitude difference as compared to the first study. The difference is likely explained by the different sequences of cTnI used, where the NMR experiment used residues $cTnI_{147−163}$, and the fluorescence experiment used $cTnI_{128−180}$. Because C-terminal residues of cTnI are largely structural,[6] the additional 17 residues located on the C-terminal end of the $cTnI_{SP}$ may significantly increase the binding affinity of $cTnI_{SP}$ to the $cTnC_{HP}$. In order for the $cTnI_{SP}$ to bind to the $cTnC_{HP}$, cTnC first needs to undergo an opening event. Although this event is difficult to measure experimentally,[32] it has been studied computationally before by Bowman et al. using a model of just the N-terminal region of cTnC.[16]

We therefore set out to estimate the free energy associated with the $cTnI_{SP}$−$cTnC_{HP}$ binding and the opening of the $cTnC_{HP}$ using a combination of MD-based simulations and free energy methods. To obtain a trajectory of conformations between the Ca^{2+}-unbound, $cTnI_{SP}$-unbound structure and the Ca^{2+}-bound, $cTnI_{SP}$-bound structure, we employed targeted molecular dynamics (TMD). This specific type of MD simulation can steer a starting model toward a target model by applying an additional potential energy function.[33] The implementation of this MD method has been shown recently to help elucidate transition pathways of other proteins.[34,35] Using the conformations along this transition, we performed US to determine the free energy associated with two separate events: opening of the $cTnC_{HP}$ and $cTnI_{SP}$ binding to $cTnC_{HP}$. We also applied this same method to mutations known to be linked with HCM or RCM, one mutation that was experimentally designed to increase Ca^{2+} sensitivity of cTnC, and the phosphorylation of cTnI Thr143. Given that Ca^{2+} binding causes opening of the $cTnC_{HP}$, we hypothesized that mutations linked with HCM or RCM and/or known to experimentally increase Ca^{2+} sensitivity would lower the free energy associated with the $cTnC_{HP}$ opening event. For the $cTnI_{SP}$−$cTnC_{HP}$ interaction, we hypothesized that these same mutations may cause the free energy of $cTnI_{SP}$−$cTnC_{HP}$ binding to become less favorable due to the mutations potentially disturbing important residue−residue contacts necessary for binding.

We were able to make two important observations from these simulations. First, our TMD method followed by US was able to calculate values for both the $cTnC_{HP}$ opening and $cTnI_{SP}$ binding free energies in agreement with previous

https://doi.org/10.1021/acs.jcim.2c00508
J. Chem. Inf. Model. 2022, 62, 5666−5674

experimental and computational studies. This agreement allowed us to conclude that our method is a reliable way to study the free energy profile of the transition between Ca^{2+}-unbound and Ca^{2+}-bound conformations of cTn. Second, we saw a general slight decrease in free energy of the $cTnC_{HP}$ opening upon introduction of mutations linked with HCM and RCM, as well as the Ca^{2+}-sensitizing mutation L48Q. However, we did not observe a general weakening or strengthening of the $cTnI_{SP}$−$cTnC_{HP}$ binding upon introduction of these same mutations.

METHODS

Model Preparation for TMD. To run TMD, a start and end point for the cTn complex simulations needed to be obtained. For the starting model, chains a, b, and c from PDB entry 6KN7[5] were extracted (Figure 1A). This model provides atom positions for all three subunits of cTn in the Ca^{2+}-unbound, $cTnI_{SP}$-unbound form in the context of the thin filament. For the end point of the TMD simulation, chains a, b, and c from PDB entry 6KN8[5] were extracted (Figure 1B). This model provides atom positions for all three subunits of cTn in the Ca^{2+}-bound, $cTnI_{SP}$-bound form in the context of the thin filament. Since TMD requires identical atoms for the start and end models, the following residues for both extracted models were used in the simulations: cTnC residues 2−161, cTnI residues 41−166, and cTnT residues 199−272. Neither of these two PDBs provided information on the position of Ca^{2+} ions, so Ca^{2+} was added to sites II, III, and IV of the cTnC in both models using AutoDock Vina.[36] Although the 6KN7 model represents a Ca^{2+}-unbound, $cTnI_{SP}$-unbound form of the cTn complex, Ca^{2+} binding initiates the conformational change to the $cTnI_{SP}$-bound form of the cTn complex, making the addition of Ca^{2+} to site II of the start model necessary to simulate the conformational change appropriately.

TMD Optimization and Simulations. For the TMD simulations, the structures were solvated with explicit TIP3W water molecules and NaCl counterions were added to neutralize the entire system and establish a final salt concentration of 150 mM. The system was minimized over two sequential 10,000 minimization steps to optimize the positions of the solvent molecules around the protein and to subsequently relax the positions of residue side-chain atoms. The system was then slowly heated up to 310 K over an initial equilibration of 190,000 steps, followed by a final equilibration of 10,000 steps, to bring the system into the final production run conditions. Pressure was controlled at atmospheric conditions during equilibration simulations using Langevin piston pressure control. All preparation steps and TMD simulations were conducted using NAMD 2.13[37] and a 2 femtosecond timestep. Parameters for all atoms within the simulation were determined from the Charmm36 force field.[38] Although previous studies have detailed difficulties of modeling Ca^{2+} ion interactions and Ca^{2+}-binding free energies in MD simulations involving biomolecules, the Charmm36 force field has been shown as a reliable force field option for producing experimental-like configurations of proteins in simulations where Ca^{2+} is bound to an EF-hand protein (i.e., troponin).[39] The TMD simulations were conducted using an NPT ensemble at 310 K with Langevin temperature and pressure dampening. All bonds with hydrogens were constrained using the ShakeH algorithm, which allowed for a 2 femtosecond timestep, with structures being saved every 2 picoseconds.

Three independent TMD simulations were performed for 60 ns using a force constant of k = 200 kcal/mol/Å^2. Technical details of TMD simulations, the process for determining optimal parameters for the cTn system, and post-simulation processing and analysis of the trajectories are described in the Supporting Information. For each frame in these trajectories, two values were determined: the interhelical distance between cTnC helices A and B and the distance between the $cTnI_{SP}$ and the cTnC hydrophobic patch. Interhelical distance was used as a proxy for interhelical angle to evaluate the degree of openness of the hydrophobic patch by measuring the distance between residues 14 and 48 of cTnC. The position of residues 14 and 48 in each frame, respectively, was determined by averaging the position of the residues' N, C, and CA atoms. The distance between the $cTnI_{SP}$ (residues 149−164) and the $cTnC_{HP}$ (residues 20, 23, 24, 26, 27, 36, 41, 44, 48, 57, 60, 77, 80, and 81) was determined by calculating the average position of the CA atoms in the collective group of residues for each region and measuring the distance between the two centers of mass. The trial that exhibited the most sampling close to the line of regression was selected as the representative trajectory from which frames were extracted to run US.

Umbrella Sampling. Specific frames from the representative TMD trajectories were selected as windows for US simulations (Table S1). The timestep for these simulations was set to 1 fs. For each US window, two independent sets of simulations were performed: one set of simulations with the $cTnC_{HP}$ interhelical distance as a collective variable and another independent set of simulations with the $cTnI_{SP}$−$cTnC_{HP}$ distance as a collective variable. The variables were defined as shown in Table S1, and a harmonic force constant of 5 kcal/mol was applied. Interhelical distance was restrained by evaluating the distance between the average position of atoms N, C, and CA in residues 14 and 48 of cTnC. The $cTnI_{SP}$−$cTnC_{HP}$ distance was restrained by evaluating the average position of the CA atoms in the collective group of residues for each region (see the TMD section above). Each of the 27 windows was then run for 8 ns in 3 independent simulations for each of the collective variables, at 310 K under an NPT ensemble, similar to the TMD simulations.

Simulations that used cTn structures with cardiomyopathic mutations, phosphorylation, or Ca^{2+}-sensitizing mutations were created by modifying the windows described above. We selected all cTn mutations in the $cTnI_{IP}$, $cTnI_{SP}$, and NcTnC regions that have been previously linked with cardiomyopathy.[2] For many of those mutations, unfortunately, there was no experimental data available on the free energy of opening the $cTnC_{HP}$ or the $cTnI_{IP}$ binding affinity. The designed L48Q mutation in the NcTnC region was included due to extensive experimental research revealing that the mutation has a Ca^{2+}-sensitizing effect.[40,41] The post-translational modification of T143 has been shown to physiologically occur and has been suggested to cause a Ca^{2+}-sensitizing effect.[42] For cardiomyopathic or Ca^{2+}-sensitizing mutations, the mutations were introduced to each window using the Mutagenesis Wizard function available in PyMOL.[43] Mutations introduced to cTnC include A8V, L29Q, A31S, L48Q, and C84Y. Mutations introduced to cTnI include R141Q, L144P, L144Q, R145G, R145Q, R145W, A157V, R162P, R162Q, and R162W. The cTnI Thr143-phosphorylated (T143p) windows were created using the PyTMs plug-in available in PyMOL.[44] Each of the modified windows was also run for 8 ns in 3 independent simulations, at 310 K under an NPT ensemble.

https://doi.org/10.1021/acs.jcim.2c00508
J. Chem. Inf. Model. 2022, 62, 5666−5674

WHAM Free Energy Estimation. For each frame in each US trajectory, the values of the applied collective variable were evaluated. The Weighted Histogram Analysis Method (WHAM)[45] was used to create a free energy profile based on the individual collective variable evaluated. This allowed us to estimate free energy profiles of the $cTnC_{HP}$ opening transition coordinate and $cTnI_{SP}$ association coordinate, respectively, without bias of the other collective variable restraining the system during simulation.

The final reported values for the free energy attributed to each collective variable were determined by averaging the data from the three independent simulations for each system, with errors being reported as the sample standard deviation between the three trials. The minimum and maximum values provided to WHAM for the interhelical distance collective variable were 14.5 and 28.5 Å, respectively. The minimum and maximum values provided to WHAM for the $cTnI_{SP}$−$cTnC_{HP}$ distance collective variable were 9.6 and 16.2 Å, respectively. The histogram analysis for both profiles was divided into 27 bins, one for each of the windows simulated, with the center of the bin being defined as the energy minimum for the window. A tolerance of 0.00001 was applied, and a force constant of 10 kcal/mol was used after properly adjusting the 5 kcal/mol spring constant applied in the Charmm36 force field. Adjustment of the spring constant for implementing WHAM was necessary because the Charmm36 force field does not include a $^2/_1$ when specifying spring constants for the restraint terms, yet the code for WHAM does. This force constant adjustment is described in "An implementation of WHAM: the Weighted Histogram Analysis Method" by Alan Grossfield.[45]

RESULTS

TMD Simulations Generate a Transition Pathway for Umbrella Sampling. TMD simulations were used to obtain a trajectory of the transition from a Ca^{2+}-unbound, $cTnI_{SP}$-unbound cTn complex to a Ca^{2+}-bound, $cTnI_{SP}$-bound cTn complex. We optimized two variables in the potential energy function for the TMD term: the force constant, k (kcal/mol/Å^2), and the length of the simulation, t. TMD simulations were run for five separate force constants, at increasing simulation lengths. For each simulation, the interhelical angle between cTnC helices A and B for all frames captured from the trajectories was determined. TMD trajectories run for t = 20 ns and t = 40 ns exhibited abnormally high interhelical angles for the lowest three force constants (k = 50 kcal/mol/Å^2, k = 100 kcal/mol/Å^2, and k = 200 kcal/mol/Å^2), while higher force constants (k = 500 kcal/mol/Å^2 and k = 1000 kcal/mol/Å^2) led to a rapid $cTnC_{HP}$ opening (Figure S1). Additionally, visual inspection for all these simulations revealed denaturation of the $cTnI_{SP}$ into a disordered region before interaction with the $cTnC_{HP}$. For the t = 60 ns simulations, the trajectories with k = 50 kcal/mol/Å^2 and k = 100 kcal/mol/Å^2 force constants again experienced unnaturally high interhelical angles. The k = 200 kcal/mol/Å^2 and k = 500 kcal/mol/Å^2 trajectories exhibited sufficient sampling of both the closed and open states of the $cTnC_{HP}$ while also sampling a smooth transition between the two (Figure 2). Visual inspection of the $cTnI_{SP}$ region revealed that $cTnI_{SP}$ maintained its helical nature for both force constants throughout the 60 ns simulation. We therefore chose to move forward with the parameters t = 60 ns and k = 200 kcal/mol/Å^2 to avoid denaturation of parts of the cTn complex. Simulations ran for t = 80 ns and t = 100 ns across all force constants also sampled the anticipated ranges of interhelical angles and exhibited gradual $cTnC_{HP}$ opening events, but we decided to use the shorter t = 60 ns simulations for production runs.

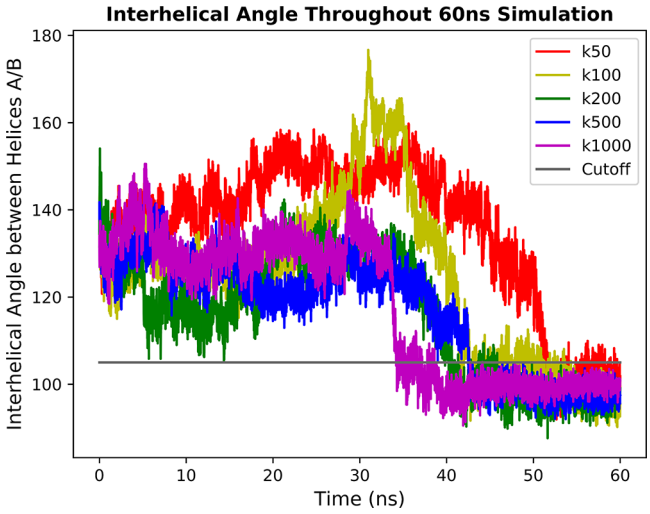

Figure 2. Interhelical angle throughout the 60 ns TMD simulations. Time of the simulation vs interhelical angle of NcTnC helices A and B. The gray "cutoff" line at the 105° mark was added to differentiate between open and closed conformations. Force constants are colored: red (k = 50 kcal/mol/Å^2), yellow (k = 100 kcal/mol/Å^2), green (k = 200 kcal/mol/Å^2), blue (k = 500 kcal/mol/Å^2), and purple (k = 1000 kcal/mol/Å^2).

Three independent trials of TMD of the WT cTn complex were run using these parameters (k = 200 kcal/mol/Å^2 and simulation length of 60 ns), and the sampling along the $cTnC_{HP}$ patch opening coordinate was investigated. The correlation between the interhelical angle and the interhelical distance for helices A/B can be seen in Figure S2. Furthermore, the data for each frame in the trajectories was analyzed with respect to the interhelical and $cTnI_{SP}$−$cTnC_{HP}$ distances, with a line of regression being created along the patch opening event (Figure 3A). To obtain full coverage of the transition coordinate between the closed and open hydrophobic patch, target values for the interhelical distance were set every 0.5 Å between 15.0 and 28.0 Å, creating 27 target interhelical distances. This corresponded to interhelical angles ranging from approximately 95 to 130°. Each of these values was paired according to the regression with a target $cTnI_{SP}$−$cTnC_{HP}$ distance to obtain full coverage of the transition coordinate between an unbound $cTnI_{SP}$ and a bound $cTnI_{SP}$. This resulted in 27 windows with pairs of target values, ranging from window 1 with a closed $cTnC_{HP}$ and unbound $cTnI_{SP}$ (interhelical distance = 15.0 Å, $cTnI_{SP}$−$cTnC_{HP}$ distance = 15.7 Å) to window 27 with an open $cTnC_{HP}$ bound to the $cTnI_{SP}$ (28.0 Å, 10.3 Å) (Figure 3B). Figure 3C−E shows the starting conformation of the cTn complex for windows 1, 14, and 27, respectively. Window 1 shows the $cTnI_{SP}$ near a closed $cTnC_{HP}$, window 9 contains the $cTnI_{SP}$ in a primed position to bind to the $cTnC_{HP}$ (while the patch is only in a semi-open conformation), and window 27 corresponds to the $cTnI_{SP}$ completely bound to an open $cTnC_{HP}$.

WT Free Energies of Patch Opening and Switch Peptide Binding Agree with Previous Experiments. For the WT system, we simulated the 27 extracted windows in triplicate for each collective variable using US and evaluated

https://doi.org/10.1021/acs.jcim.2c00508
J. Chem. Inf. Model. 2022, 62, 5666−5674

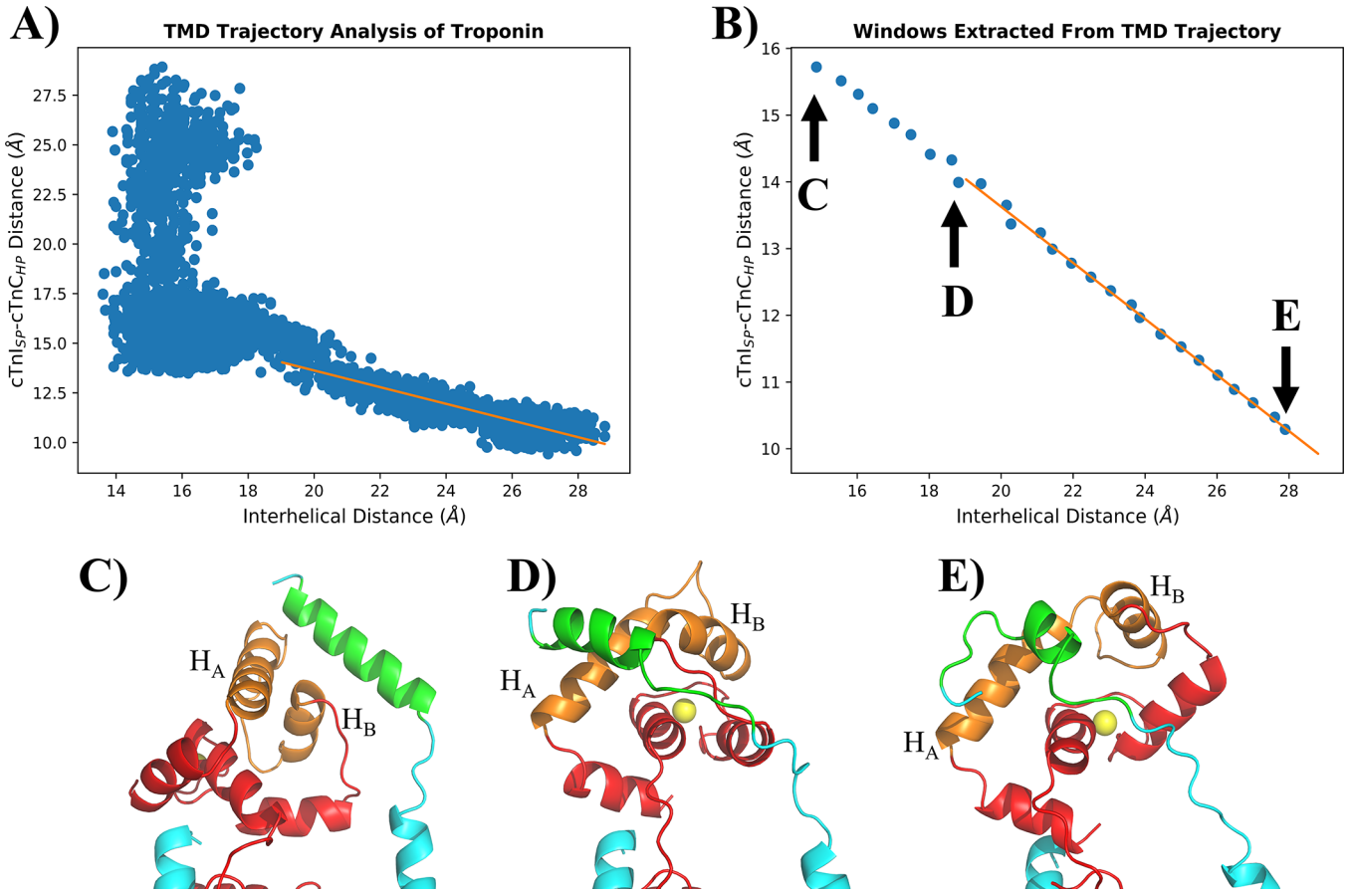

Figure 3. TMD trajectory analysis and window extraction. A) Each point represents a frame from the TMD trajectory. Line of regression was created using all data points where the interhelical distance is ≥19.0 Å. B) Each point represents one of the 27 windows extracted for input of US. The same line of regression from (A) is shown in orange. Simulation windows shown in (C), (D), and (E) are labeled with arrows. C) Window 1 with an interhelical distance of 15.0 Å and a $cTnI_{SP}$–$cTnC_{HP}$ distance of 15.8 Å. This window has the $cTnI_{SP}$ near a closed $cTnC_{HP}$ and represents the start point of the transition coordinate. D) Window 9 with an interhelical distance of 19.0 Å and a $cTnI_{SP}$–$cTnC_{HP}$ distance of 14.1 Å. This window has the $cTnI_{SP}$ in a primed position to bind to the $cTnC_{HP}$; however, the patch is only in a semi-open conformation. E) Window 27 with an interhelical distance of 28.0 Å and a $cTnI_{SP}$–$cTnC_{HP}$ distance of 10.3 Å. This window has the $cTnI_{SP}$ completely bound to an open $cTnC_{HP}$ and represents the end point of the transition coordinate. All regions of the cTn complex are colored identical to Figure 1. cTnC helices A and B (orange) labeled as H_A and H_B, respectively.

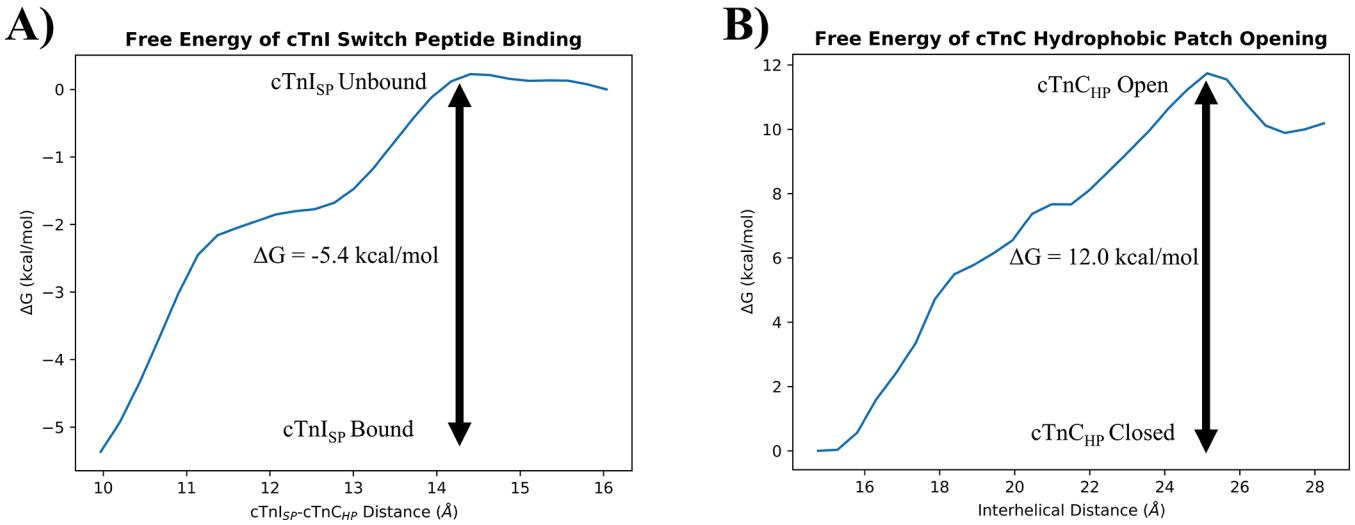

Figure 4. WHAM calculated free energy of WT transition coordinates. A) The free energy across the $cTnI_{SP}$–$cTnC_{HP}$ binding coordinate for the WT cTn model. Binding occurs right (window 7) to left (window 27) as the distance between the two entities decreases. B) The free energy across the $cTnC_{HP}$ opening coordinate. The $cTnC_{HP}$ opens from left (window 1) to right (window 27).

https://doi.org/10.1021/acs.jcim.2c00508
J. Chem. Inf. Model. 2022, 62, 5666−5674

the results with WHAM. We created a free energy profile considering each collective variable independently (Figure 4). Analysis of the US simulations revealed that the evenly spaced windows exhibited sufficient overlap and that we were able to sample the entire reaction coordinate (Figure S3). Evaluating the convergence of the free energy calculated by WHAM as a function of simulation time revealed that 8 ns was sufficient for sampling the windows of both collective variables (Figure S4). The free energy estimated for the $cTnI_{SP}$ binding event only fluctuated by about 0.1 kcal/mol after 5 ns (Figure S4A), and the $cTnC_{HP}$ opening free energy only changed by 0.3 kcal/mol after 5 ns (Figure S4B). The estimated free energy of the $cTnI_{SP}$−$cTnC_{HP}$ binding event was then determined to be −5.4 ± 0.5 kcal/mol. Figure 4A shows the calculated free energy per window as a function of the distance between the $cTnI_{SP}$ and $cTnC_{HP}$. The free energy was measured from the peak of the free energy curve in window 7 (the unbound state; at a $cTnI_{SP}$−$cTnC_{HP}$ distance of about 14.5 Å) to the free energy estimation in the last window (the bound state; at a $cTnI_{SP}$−$cTnC_{HP}$ distance of about 10.3 Å; window 27). This was done because the $cTnI_{SP}$ was not in proximity to the $cTnC_{HP}$ binding site until window 7, when the patch opening reached a semi-open conformation suitable for $cTnI_{SP}$−$cTnC_{HP}$ binding to commence.

An NMR kinetic study of $cTnI_{147-163}$ titrated to a Ca^{2+}-bound NcTnC estimated a binding K_D of 154 ± 10 μM.[30] This experimental study is the most comparable to our simulation data because a highly similar region for the $cTnI_{SP}$ was used. At T = 303.15 K (30 °C), this data corresponds to an experimentally determined free energy of −5.3 ± 0.1 kcal/mol, a value in perfect agreement with our computational value of −5.4 ± 0.5 kcal/mol. Other experimental studies explored the binding of longer cTnI segments to cTnC. However, since residues located C-terminally of the $cTnI_{SP}$ were not resolved in the 6KN8 PDB structure, we were unable to test the effect of these residues on the switch peptide binding affinity. Given this small deviation, we hypothesized that our method of using TMD to produce windows representative of a transition coordinate, in combination with US to measure the free energy along that coordinate, can reliably reproduce experimentally determined free energy values of events associated with the cTn conformational transition. Applying the same strategy to the $cTnC_{HP}$ opening transition coordinate, we estimated the free energy of the opening event to be 12.0 ± 1.3 kcal/mol. The WHAM determined free energy as a function of the opening coordinate can be seen in Figure 4B. Although the free energy of this event has not been studied experimentally, the result agrees with previous computational simulations that measured the free energy of $cTnC_{HP}$ opening in NcTnC to be 13.8 ± 2.2 kcal/mol using a combination of steered MD and US.[16]

To test the effect of the $cTnI_{SP}$ getting incrementally closer to a closed hydrophobic patch, we extracted 11 windows from our TMD simulations (each at a $cTnC_{HP}$ interhelical distance of 15 Å), with a decreasing $cTnI_{SP}$−$cTnC_{HP}$ distance between 25 and 20 Å (step size 0.5 Å). Between these windows, we observed only a small change in free energy (∼1.8 kcal/mol) as the $cTnI_{SP}$ shifted its position closer to the $cTnC_{HP}$ (Figure S5). We would not expect this small difference to significantly affect the reported results.

HCM and RCM Mutations Generally Decreased $cTnC_{HP}$ Opening Free Energy. After developing a reliable method to measure the free energy of the $cTnC_{HP}$ opening and $cTnI_{SP}$−$cTnC_{HP}$ binding events, we subsequently introduced mutations and post-translational modifications in cTn to determine how these changes affect the free energies of patch opening and switch peptide binding. We tested 12 mutations that have been linked with HCM, two mutations linked with RCM, one designed mutation that increases Ca^{2+} sensitivity without causing disease, and phosphorylation of cTnI Thr143. All modifications tested were located in the NcTnC region or between residues 141−162 of cTnI. Data for the estimated free energy of patch opening and switch peptide binding for all 16 modified systems can be seen in Table 1.

Table 1. Free Energy of $cTnC_{HP}$ Opening and $cTnI_{SP}$ Binding Events for All Models. All data shown in units of kcal/mol.

Model	Disease	ΔG $cTnC_{HP}$ Opening	ΔG $cTnI_{SP}$ Binding
Wild-Type	---	12.0 ± 1.3	-5.4 ± 0.5
cTnC A8V	HCM	11.6 ± 1.7	-3.9 ± 1.3
cTnC L29Q	HCM	13.1 ± 1.8	-7.2 ±1.2
cTnC A31S	HCM	11.4 ± 1.0	-4.3 ± 1.0
cTnC L48Q	---	4.8 ± 1.5	-8.0 ± 0.2
cTnC C84Y	HCM	8.4 ± 1.1	-6.4 ± 0.6
cTnI R141Q	HCM	13.6 ± 0.7	-4.3 ± 0.7
cTnI L144P	HCM	12.3 ± 2.2	-3.6 ± 1.5
cTnI R145G	HCM	12.5 ± 1.0	-5.5 ± 1.0
cTnI R145Q	HCM	13.5 ± 2.5	-7.2 ± 0.6
cTnI A157V	HCM	12.5 ± 1.9	-5.6 ± 2.2
cTnI R162P	HCM	12.6 ± 2.5	-3.5 ± 1.1
cTnI R162Q	HCM	11.4 ± 1.8	-4.3 ± 0.9
cTnI R162W	HCM	11.8 ± 0.9	-4.4 ± 1.3
cTnI L144Q	RCM	11.7 ± 2.5	-4.7 ± 0.5
cTnI R145W	RCM	10.4 ± 1.8	-5.6 ± 1.0
cTnI T143p	---	15.6 ± 0.9	-4.6 ± 1.5

Two of the mutations (cTnC L48Q and C84Y) exhibited a significant decrease in the free energy of $cTnC_{HP}$ opening (Figure 5A), while the other 13 mutations caused no significant change in the free energy.

Two mutations had a drastic effect on the $cTnC_{HP}$ opening: L48Q (4.8 kcal/mol) and C84Y (8.4 kcal/mol). Interestingly, the mutation that caused the biggest change in free energy of this opening event was L48Q, a designed cTnC Ca^{2+}-sensitizing mutation that has not been linked with disease.[40,41] This mutation also caused the most favorable $cTnI_{SP}$−$cTnC_{HP}$ interaction (−8.0 kcal/mol) among all mutations studied (see the next section). The only cardiomyopathic mutation that we observed having a significant effect on the $cTnC_{HP}$ opening was cTnC C84Y. This mutation has been shown experimentally to increase Ca^{2+} sensitivity of force generation in skinned cardiac muscle fibers.[46]

Mutations in the cTnI inhibitory peptide and $cTnI_{SP}$ regions did not affect the free energy of $cTnC_{HP}$ opening significantly. Prior experiments have suggested that cTnI mutations that cause a more severe increase in Ca^{2+} sensitivity lead to RCM, whereas mutations that cause a less severe increase in Ca^{2+} sensitivity lead to HCM.[47] Our data would support this theory since mutations linked with RCM in the cTnI inhibitory peptide and $cTnI_{SP}$ regions (L144Q and R145W) generally had a larger effect on the $cTnC_{HP}$ opening free energy when compared to HCM mutations in the same region. Currently, no RCM mutations have been identified in cTnC,[2,48] so we were unable to test this trend among the cTnC mutations.

https://doi.org/10.1021/acs.jcim.2c00508
J. Chem. Inf. Model. 2022, 62, 5666−5674

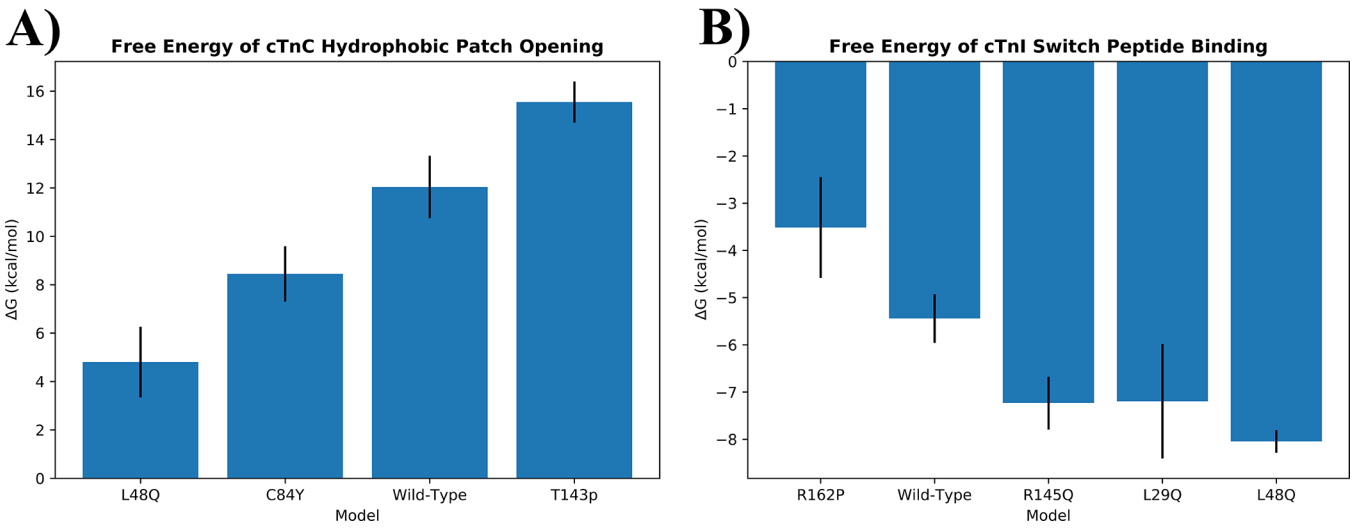

Figure 5. Free energy of $cTnC_{HP}$ opening and $cTnI_{SP}$ binding events for all simulated systems that caused a significant impact. A) WHAM calculated ΔG for the $cTnC_{HP}$ opening event for cTn systems ordered based on average ΔG. B) WHAM calculated ΔG for the $cTnI_{SP}$ binding event for cTn systems ordered based on average ΔG. The standard deviations for each system are shown as black bars.

No Observed Trend in $cTnI_{SP}$–$cTnC_{HP}$ Binding Free Energy. We were unable to observe any consistent trend in the free energy of $cTnI_{SP}$–$cTnC_{HP}$ binding. Three mutations (cTnC L29Q, cTnC L48Q, and cTnI R145Q) caused a significantly more favorable interaction, one mutation (cTnI R162P) caused a less favorable interaction, and the other eleven mutations had no measurable effect on $cTnI_{SP}$–$cTnC_{HP}$ binding (Figure 5B and Table 1). The effect of cTn mutations on $cTnI_{SP}$–$cTnC_{HP}$ binding has been scarcely studied before. A study by Tikunova et al. that estimated the binding affinity of $cTnI_{128-180}$ to cTnC in the presence of Ca^{2+}-sensitizing, non-cardiomyopathic mutations observed a slight increase in K_D when compared to the WT.[31] We would therefore hypothesize to see a less favorable interaction between the $cTnI_{SP}$ and the $cTnC_{HP}$ given mutations linked with HCM or RCM or those that have been experimentally shown to cause a Ca^{2+}-sensitizing effect. Although we did observe slightly less favorable interactions in most of the mutated models, only one model produced a significantly less favorable interaction. For the one Ca^{2+}-sensitizing, non-cardiomyopathic mutation that was studied (L48Q), we observed a significantly more favorable $cTnI_{SP}$–$cTnC_{HP}$ interaction (−8.0 kcal/mol) as compared to WT. Interestingly, the other cTnC mutation that caused a more favorable interaction (L29Q) was also a leucine to glutamine substitution.

Thr143 Phosphorylation May Increase $cTnC_{HP}$ Opening Free Energy. PKA-mediated phosphorylation of cTnI has been shown as a mechanism for increasing the heart rate under stress by allowing the heart muscle to contract at a faster rate as a consequence of a decrease in Ca^{2+} sensitivity from phosphorylation of cTnI Ser 22/23.[49] However, studies of the PKC-mediated phosphorylation of cTnI Thr143 have actually shown the adverse effect, namely, that phosphorylation of this site may cause an increase in Ca^{2+} sensitivity in the myofilament.[42] Our phosphorylated model of cTnI Thr143 (cTnI T143p) slightly increased the $cTnC_{HP}$ opening free energy (15.6 kcal/mol) while having no effect on the free energy of $cTnI_{SP}$–$cTnC_{HP}$ binding. Therefore, our simulations suggested that the phosphorylation of cTnI T143 might decrease calcium sensitivity through an increase in the free energy of $cTnC_{HP}$ opening. A possible explanation for this apparent inconsistency with the experimentally observed increase in Ca^{2+} sensitivity was highlighted in a study by Vyměťal et al.[50] The authors showed that current force fields were unable to simulate phosphorylated residues in a way that would agree with experimental observations. Therefore, the phosphorylated Thr143 in our cTn system was most likely behaving uncharacteristically, leading to results that did not corroborate experimental data.

CONCLUSIONS

In this study, we modeled the transition of cTn from the Ca^{2+}-unbound to Ca^{2+}-bound states by using TMD. Using the trajectory of this transition, we subsequently performed US simulations to determine the free energy associated with two separate events: opening of the $cTnC_{HP}$ and $cTnI_{SP}$ binding to $cTnC_{HP}$. The results obtained for the $cTnI_{SP}$–$cTnC_{HP}$ interaction in the WT model agreed with previous experimental results,[30] while our $cTnC_{HP}$ opening free energy estimation agreed with previous computational efforts.[16] This excellent agreement for WT cTn demonstrates the important role of advanced computational methods in quantitatively studying cTn dynamics and muscle contraction. The methodology described here, using TMD followed by US, could also be applied to other protein systems given the availability of structures in two different states.

We further applied the methodology to cTn mutations and post-translational modifications. Our results showed that mutations linked with HCM or RCM caused a Ca^{2+}-sensitizing effect, generally lowering the free energy associated with the $cTnC_{HP}$ opening. We observed that most of the studied mutations caused a less favorable free energy associated with $cTnI_{SP}$–$cTnC_{HP}$ binding, although this trend did not hold for all HCM and RCM mutations, with three mutations leading to significantly more favorable binding free energies for this event. Our method could impact the future of computational studies on this system by predicting the consequences of unknown mutations on cTn energetics. Additionally, this method could prove helpful in rational protein design. Overall, we showed that our protocol of utilizing US to measure the free energy of transitions sampled by TMD is a reliable method for studying the energetics of the cTn complex.

https://doi.org/10.1021/acs.jcim.2c00508
J. Chem. Inf. Model. 2022, 62, 5666−5674

■ ASSOCIATED CONTENT

Data Availability Statement

The wild-type cTn protein structures (6KN7, 6KN8) were available in the Protein Data Bank (PDB) at https://www.rcsb.org/. All mutations were created using the wild-type protein structure as the base model within the PyMOL software using the protein mutagenesis tool. Phosphorylation was created using the wild-type protein structure as the base model within the PyMOL software using the PyTMs Plug-in. All TMD and US simulations were performed within the NAMD version 2.13 framework. Weighted Histogram Analysis Method (WHAM) was performed using WHAM version 2.0.11 available at http://membrane.urmc.rochester.edu/?page_id=126.

Supporting Information

The Supporting Information is available free of charge at https://pubs.acs.org/doi/10.1021/acs.jcim.2c00508.

Methods for optimization of TMD simulation parameters, values for collective variables used for each window in US, interhelical angle analysis during TMD simulations, comparison of interhelical angle vs interhelical distance, coverage of collective variables in US simulations, free energy convergence of US simulations, and free energy analysis of $cTnI_{SP}$ approaching a closed $cTnC_{HP}$ (PDF)

■ AUTHOR INFORMATION

Corresponding Author

Steffen Lindert − *Department of Chemistry and Biochemistry, The Ohio State University, Columbus, Ohio 43210, United States;* orcid.org/0000-0002-3976-3473; Phone: 614-292-8284; Email: lindert.1@osu.edu; Fax: 614-292-1685

Author

Austin M. Cool − *Department of Chemistry and Biochemistry, The Ohio State University, Columbus, Ohio 43210, United States*

Complete contact information is available at: https://pubs.acs.org/10.1021/acs.jcim.2c00508

Notes

The authors declare no competing financial interest.

■ ACKNOWLEDGMENTS

The authors would like to thank Marcos Sotomayor for sharing his expertise with respect to applying external forces in MD simulations, Jon Davis for his insight into previous experimental procedures related to the work, as well as members of the Lindert Lab for their discussions and suggestions. Additionally, we would like to thank the Ohio Supercomputer Center[51] for valuable computational resources. This work was supported by the NIH (R01 HL137015 to S.L.).

■ REFERENCES

(1) Marston, S.; Zamora, J. E. Troponin structure and function: a view of recent progress. *J. Muscle Res. Cell Motil.* **2020**, 1−19.

(2) Lu, Q. W.; Wu, X. Y.; Morimoto, S. Inherited cardiomyopathies caused by troponin mutations. *J. Geriatr. Cardiol.* **2013**, *10*, 91−101.

(3) Ciarambino, T.; Menna, G.; Sansone, G.; Giordano, M. Cardiomyopathies: An Overview. *Int. J. Mol. Sci.* **2021**, *22*, 7722.

(4) Takeda, S.; Yamashita, A.; Maeda, K.; Maéda, Y. Structure of the core domain of human cardiac troponin in the Ca(2+)-saturated form. *Nature* **2003**, *424*, 35−41.

(5) Yamada, Y.; Namba, K.; Fujii, T. Cardiac muscle thin filament structures reveal calcium regulatory mechanism. *Nat. Commun.* **2020**, *11*, 1−9.

(6) Bowman, J. D.; Lindert, S. Computational Studies of Cardiac and Skeletal Troponin. *Front. Mol. Biosci.* **2019**, *6*, 68.

(7) Lindert, S.; Kekenes-Huskey, P. M.; Huber, G.; Pierce, L.; McCammon, J. A. Dynamics and calcium association to the N-terminal regulatory domain of human cardiac troponin C: a multiscale computational study. *J. Phys. Chem. B* **2012**, *116*, 8449−8459.

(8) Rayani, K.; Seffernick, J.; Li, A. Y.; Davis, J. P.; Spuches, A. M.; Van Petegem, F.; Solaro, R. J.; Lindert, S.; Tibbits, G. F. Binding of calcium and magnesium to human cardiac troponin C. *J. Biol. Chem.* **2021**, *296*, No. 100350.

(9) Hantz, E. R.; Lindert, S. Adaptative Steered Molecular Dynamics Study of Mutagenesis Effects on Calcium Affinity in the Regulatory Domain of Cardiac Troponin C. *J. Chem. Inf. Model.* **2021**, *61*, 3052−3057.

(10) Rayani, K.; Hantz, E. R.; Haji-Ghassemi, O.; Li, A. Y.; Spuches, A. M.; Van Petegem, F.; Solaro, R. J.; Lindert, S.; Tibbits, G. F. The effect of Mg(2+) on Ca(2+) binding to cardiac troponin C in hypertrophic cardiomyopathy associated TNNC1 variants. *FEBS J.* 2022, DOI: 10.1111/febs.16578.

(11) Votapka, L. W.; Amaro, R. E. Multiscale Estimation of Binding Kinetics Using Brownian Dynamics, Molecular Dynamics and Milestoning. *PLoS Comput. Biol.* **2015**, *11*, No. e1004381.

(12) Kekenes-Huskey, P. M.; Lindert, S.; McCammon, J. A. Molecular basis of calcium-sensitizing and desensitizing mutations of the human cardiac troponin C regulatory domain: a multi-scale simulation study. *PLoS Comput. Biol.* **2012**, *8*, No. e1002777.

(13) Dewan, S.; McCabe, K. J.; Regnier, M.; McCulloch, A. D.; Lindert, S. Molecular Effects of cTnC DCM Mutations on Calcium Sensitivity and Myofilament Activation-An Integrated Multiscale Modeling Study. *J. Phys. Chem. B* **2016**, *120*, 8264−8275.

(14) Stevens, C. M.; Rayani, K.; Singh, G.; Lotfalisalmasi, B.; Tieleman, D. P.; Tibbits, G. F. Changes in the dynamics of the cardiac troponin C molecule explain the effects of Ca. *J. Biol. Chem.* **2017**, *292*, 11915−11926.

(15) Lindert, S.; Kekenes-Huskey, P. M.; McCammon, J. A. Long-timescale molecular dynamics simulations elucidate the dynamics and kinetics of exposure of the hydrophobic patch in troponin C. *Biophys. J.* **2012**, *103*, 1784−1789.

(16) Bowman, J. D.; Lindert, S. Molecular Dynamics and Umbrella Sampling Simulations Elucidate Differences in Troponin C Isoform and Mutant Hydrophobic Patch Exposure. *J. Phys. Chem. B* **2018**, *122*, 7874−7883.

(17) Bowman, J. D.; Coldren, W. H.; Lindert, S. Mechanism of Cardiac Troponin C Calcium Sensitivity Modulation by Small Molecules Illuminated by Umbrella Sampling Simulations. *J. Chem. Inf. Model.* **2019**, *59*, 2964−2972.

(18) Zamora, J. E.; Papadaki, M.; Messer, A. E.; Marston, S. B.; Gould, I. R. Troponin structure: its modulation by Ca(2+) and phosphorylation studied by molecular dynamics simulations. *Phys. Chem. Chem. Phys.* **2016**, *18*, 20691−20707.

(19) Cool, A. M.; Lindert, S. Computational Methods Elucidate Consequences of Mutations and Post-translational Modifications on Troponin I Effective Concentration to Troponin C. *J. Phys. Chem. B* **2021**, *125*, 7388−7396.

(20) Rao, V.; Cheng, Y.; Lindert, S.; Wang, D.; Oxenford, L.; McCulloch, A. D.; McCammon, J. A.; Regnier, M. PKA phosphorylation of cardiac troponin I modulates activation and relaxation kinetics of ventricular myofibrils. *Biophys. J.* **2014**, *107*, 1196−1204.

(21) Cheng, Y.; Lindert, S.; Kekenes-Huskey, P.; Rao, V. S.; Solaro, R. J.; Rosevear, P. R.; Amaro, R.; McCulloch, A. D.; McCammon, J. A.; Regnier, M. Computational studies of the effect of the S23D/

S24D troponin I mutation on cardiac troponin structural dynamics. *Biophys. J.* **2014**, *107*, 1675−1685.
(22) Lindert, S.; Cheng, Y.; Kekenes-Huskey, P.; Regnier, M.; McCammon, J. A. Effects of HCM cTnI mutation R145G on troponin structure and modulation by PKA phosphorylation elucidated by molecular dynamics simulations. *Biophys. J.* **2015**, *108*, 395−407.
(23) Cheng, Y.; Rao, V.; Tu, A. Y.; Lindert, S.; Wang, D.; Oxenford, L.; McCulloch, A. D.; McCammon, J. A.; Regnier, M. Troponin I Mutations R146G and R21C Alter Cardiac Troponin Function, Contractile Properties, and Modulation by Protein Kinase A (PKA)-mediated Phosphorylation. *J. Biol. Chem.* **2015**, *290*, 27749−27766.
(24) Cheng, Y.; Lindert, S.; Oxenford, L.; Tu, A. Y.; McCulloch, A. D.; Regnier, M. Effects of Cardiac Troponin I Mutation P83S on Contractile Properties and the Modulation by PKA-Mediated Phosphorylation. *J. Phys. Chem. B* **2016**, *120*, 8238−8253.
(25) Lindert, S.; Li, M. X.; Sykes, B. D.; McCammon, J. A. Computer-aided drug discovery approach finds calcium sensitizer of cardiac troponin. *Chem. Biol. Drug Des.* **2015**, *85*, 99−106.
(26) Cai, F.; Li, M. X.; Pineda-Sanabria, S. E.; Gelozia, S.; Lindert, S.; West, F.; Sykes, B. D.; Hwang, P. M. Structures reveal details of small molecule binding to cardiac troponin. *J. Mol. Cell. Cardiol.* **2016**, *101*, 134−144.
(27) Aprahamian, M. L.; Tikunova, S. B.; Price, M. V.; Cuesta, A. F.; Davis, J. P.; Lindert, S. Successful Identification of Cardiac Troponin Calcium Sensitizers Using a Combination of Virtual Screening and ROC Analysis of Known Troponin C Binders. *J. Chem. Inf. Model.* **2017**, *57*, 3056−3069.
(28) Coldren, W. H.; Tikunova, S. B.; Davis, J. P.; Lindert, S. Discovery of Novel Small-Molecule Calcium Sensitizers for Cardiac Troponin C: A Combined Virtual and Experimental Screening Approach. *J. Chem. Inf. Model.* **2020**, *60*, 3648−3661.
(29) Varughese, J. F.; Baxley, T.; Chalovich, J. M.; Li, Y. A computational and experimental approach to investigate bepridil binding with cardiac troponin. *J. Phys. Chem. B* **2011**, *115*, 2392−2400.
(30) Li, M. X.; Saude, E. J.; Wang, X.; Pearlstone, J. R.; Smillie, L. B.; Sykes, B. D. Kinetic studies of calcium and cardiac troponin I peptide binding to human cardiac troponin C using NMR spectroscopy. *Eur. Biophys. J.* **2002**, *31*, 245−256.
(31) Tikunova, S. B.; Liu, B.; Swindle, N.; Little, S. C.; Gomes, A. V.; Swartz, D. R.; Davis, J. P. Effect of calcium-sensitizing mutations on calcium binding and exchange with troponin C in increasingly complex biochemical systems. *Biochemistry* **2010**, *49*, 1975−1984.
(32) Cordina, N. M.; Liew, C. K.; Potluri, P. R.; Curmi, P. M.; Fajer, P. G.; Logan, T. M.; Mackay, J. P.; Brown, L. J. Ca2+−induced PRE-NMR changes in the troponin complex reveal the possessive nature of the cardiac isoform for its regulatory switch. *PLoS One* **2014**, *9*, No. e112976.
(33) Schlitter, J.; Engels, M.; Krüger, P. Targeted molecular dynamics: a new approach for searching pathways of conformational transitions. *J. Mol. Graph.* **1994**, *12*, 84−89.
(34) Ermakova, E.; Kurbanov, R. Molecular insight into conformational transformation of human glucokinase: conventional and targeted molecular dynamics. *J. Biomol. Struct. Dyn.* **2020**, *38*, 3035−3045.
(35) Wolf, S.; Amaral, M.; Lowinski, M.; Vallée, F.; Musil, D.; Güldenhaupt, J.; Dreyer, M. K.; Bomke, J.; Frech, M.; Schlitter, J.; Gerwert, K. Estimation of Protein-Ligand Unbinding Kinetics Using Non-Equilibrium Targeted Molecular Dynamics Simulations. *J. Chem. Inf. Model.* **2019**, *59*, 5135−5147.
(36) Trott, O.; Olson, A. J. AutoDock Vina: improving the speed and accuracy of docking with a new scoring function, efficient optimization, and multithreading. *J. Comput. Chem.* **2010**, *31*, 455−461.
(37) Phillips, J. C.; Braun, R.; Wang, W.; Gumbart, J.; Tajkhorshid, E.; Villa, E.; Chipot, C.; Skeel, R. D.; Kalé, L.; Schulten, K. Scalable molecular dynamics with NAMD. *J. Comput. Chem.* **2005**, *26*, 1781−1802.
(38) Huang, J.; MacKerell, A. D. CHARMM36 all-atom additive protein force field: validation based on comparison to NMR data. *J. Comput. Chem.* **2013**, *34*, 2135−2145.
(39) Tan, Q.; Ding, Y.; Qiu, Z.; Huang, J. Binding Energy and Free Energy of Calcium Ion to Calmodulin EF-Hands with the Drude Polarizable Force Field. *ACS Phys. Chem. Au* **2022**, *2*, 143−155.
(40) Wang, D.; Robertson, I. M.; Li, M. X.; McCully, M. E.; Crane, M. L.; Luo, Z.; Tu, A. Y.; Daggett, V.; Sykes, B. D.; Regnier, M. Structural and functional consequences of the cardiac troponin C L48Q Ca(2+)-sensitizing mutation. *Biochemistry* **2012**, *51*, 4473−4487.
(41) Shettigar, V.; Zhang, B.; Little, S. C.; Salhi, H. E.; Hansen, B. J.; Li, N.; Zhang, J.; Roof, S. R.; Ho, H. T.; Brunello, L.; Lerch, J. K.; Weisleder, N.; Fedorov, V. V.; Accornero, F.; Rafael-Fortney, J. A.; Gyorke, S.; Janssen, P. M.; Biesiadecki, B. J.; Ziolo, M. T.; Davis, J. P. Rationally engineered Troponin C modulates in vivo cardiac function and performance in health and disease. *Nat. Commun.* **2016**, *7*, 10794.
(42) Wang, H.; Grant, J. E.; Doede, C. M.; Sadayappan, S.; Robbins, J.; Walker, J. W. PKC-betaII sensitizes cardiac myofilaments to Ca2+ by phosphorylating troponin I on threonine-144. *J. Mol. Cell. Cardiol.* **2006**, *41*, 823−833.
(43) *The PyMOL Molecular Graphics System, Version 2.0* Schrödinger, LLC.
(44) Warnecke, A.; Sandalova, T.; Achour, A.; Harris, R. A. PyTMs: a useful PyMOL plugin for modeling common post-translational modifications. *BMC Bioinform.* **2014**, *15*, 370.
(45) Grossfield, Alan, *"WHAM: the weighted histogram analysis method," version 2.0.11*, http://membrane.urmc.rochester.edu/wordpress/?page_id=126.
(46) Landstrom, A. P.; Parvatiyar, M. S.; Pinto, J. R.; Marquardt, M. L.; Bos, J. M.; Tester, D. J.; Ommen, S. R.; Potter, J. D.; Ackerman, M. J. Molecular and functional characterization of novel hypertrophic cardiomyopathy susceptibility mutations in TNNC1-encoded troponin C. *J. Mol. Cell. Cardiol.* **2008**, *45*, 281−288.
(47) Yumoto, F.; Lu, Q. W.; Morimoto, S.; Tanaka, H.; Kono, N.; Nagata, K.; Ojima, T.; Takahashi-Yanaga, F.; Miwa, Y.; Sasaguri, T.; Nishita, K. Drastic Ca2+ sensitization of myofilament associated with a small structural change in troponin I in inherited restrictive cardiomyopathy. *Biochem. Biophys. Res. Commun.* **2005**, *338*, 1519−1526.
(48) Willott, R. H.; Gomes, A. V.; Chang, A. N.; Parvatiyar, M. S.; Pinto, J. R.; Potter, J. D. Mutations in Troponin that cause HCM, DCM AND RCM: what can we learn about thin filament function? *J. Mol. Cell. Cardiol.* **2010**, *48*, 882−892.
(49) Dong, W. J.; Jayasundar, J. J.; An, J.; Xing, J.; Cheung, H. C. Effects of PKA phosphorylation of cardiac troponin I and strong crossbridge on conformational transitions of the N-domain of cardiac troponin C in regulated thin filaments. *Biochemistry* **2007**, *46*, 9752−9761.
(50) Vymětal, J.; Jurásková, V.; Vondrášek, J. AMBER and CHARMM Force Fields Inconsistently Portray the Microscopic Details of Phosphorylation. *J. Chem. Theory Comput.* **2019**, *15*, 665−679.
(51) Center, O. S. *Ohio Supercomputer Center*. 1987.

https://doi.org/10.1021/acs.jcim.2c00508
J. Chem. Inf. Model. 2022, 62, 5666−5674